Available online at www.sciencedirect.com

SciVerse ScienceDirect

Ceramics International 39 (2013) 897–901

CERAMICS INTERNATIONAL

www.elsevier.com/locate/ceramint

Short communication

ZrB_2–Al_3BC_3 composites prepared using Al–B_4C–C additives and spark plasma sintering

Hailong Wang[a,b,*], Lun Feng[a], Sea-Hoon Lee[b], Jianbao Chen[a], Bingbing Fan[a], Deliang Chen[a], Hongxia Lu[a], Hongliang Xu[a], Rui Zhang[a,c]

[a]School of Materials Science and Engineering, Zhengzhou University, Zhengzhou 450001, China
[b]Korea Institute of Materials Science, Republic of Korea
[c]Zhengzhou Institute of Aeronautical Industry Management, Zhengzhou 450015, China

Received 4 June 2012; received in revised form 20 June 2012; accepted 20 June 2012
Available online 4 July 2012

Abstract

Al_3BC_3 was fabricated by in-situ reaction of Al, B_4C and activated carbon additives, which improved both sinterability and mechanical properties of the ZrB_2 ceramics. The densification of ZrB_2 was nearly completed at 1700° C using spark plasma sintering (SPS). Both fracture toughness and flexural strength of ZrB_2 ceramics increased with the content of sintering additives, which respectively reached a maximum of 6.17 MPa $m^{1/2}$ and 529 MPa at 15 wt% ABC content.

Keywords: C. Mechanical properties; Zirconium diboride; Spark plasma sintering

1. Introduction

Due to its excellent thermal and mechanical properties, zirconium diboride (ZrB_2) is one of the most attractive materials for applications in aerospace. ZrB_2 or ZrB_2 based composites can be used as leading edges and nose caps in hypersonic re-entry space vehicles, rocket nozzle inserts and air-augmented propulsion system components [1–3]. However, the sintering of ZrB_2 ceramics is difficult, owing to the high melting point, the strong covalent bonding and low self-diffusion coefficients [4, 5]. Recently, many works have been carried out to improve the sinterability of ZrB_2. One promising approach for promoting densification is the application of sintering additives to ZrB_2. For example, the addition of metals (e.g., Ni, Fe, Mo) and ceramics (e.g., SiC, $MoSi_2$, $ZrSi_2$, Si_3N_4, AlN, ZrN) can significantly promote densification and induce microstructure through liquid-phase sintering at temperatures lower than those necessary for undoped compositions [6–10]. Another approach to enhance densification is the use of pressure- or field-assisted sintering techniques, such as hot pressing, spark plasma sintering, and microwave sintering. Among the techniques, spark plasma sintering (SPS) has been intensively used for sintering ZrB_2 ceramics in recent years due to the combination of unique properties such as fast heating/cooling rate and high applicable pressure [11–13].

In recently years, Al–B–C system (mixture of Al, B_4C, and C) has been used as efficient sintering additives of SiC because it reduces the densification temperature and improves the fracture toughness of SiC [14,15]. Liquid phase sintering was the main densification mechanism of SiC containing Al_3BC_3 additive. Al_2O_3 and B_2O_3 at the surface of Al_3BC_3 reacted with SiO_2 to form a liquid silicate phase, which caused the rearrangement and anisotropic growth of SiC grains [16]. Anisotropic growth rates of hexagonal a-SiC results in the formation of platelike and elongated grains, which can bridge the crack and shield the crack tip from the applied stress [17–19]. As Al_3BC_3 do not melt up to 2100° C, the fracture toughness of Al_3BC_3–SiC composites was found to be slightly decreased at temperatures up to 1300° C [15,20]. The result

*Corresponding author at: School of Materials Science and Engineering, Zhengzhou University, Zhengzhou 450001, China
E-mail address: 119whl@zzu.edu.cn (H. Wang).

0272-8842/$36.00
http://dx.doi.org/10.1016/j.ceramint.2012.06.064

indicated that Al–B–C system (here after termed ABC) is a potential additive for lowering the sintering temperature and improving the toughness of ZrB_2. However, researches on the sintering performance and properties of the ZrB_2–ABC systems have not been reported.

In the present study, the densification behavior of the ZrB_2-based ceramics containing 5–15 wt% ABC additives during spark plasma sintering (SPS) was investigated and the microstructure and mechanical properties of the sintered ZrB_2 were analyzed.

2. Experimental procedures

2.1. Powder preparation

Commercially available ZrB_2 (1–2 μm, purity > 99%; Alfa Aesar, MA, USA), Al (APS 11 μm, purity 99.7%; Alfa Aesar, MA, USA), B_4C (purity 99%, particle size < 10 μm; Alfa Aesar, MA, USA) and carbon black powers (S.A. 60–80 m^2/g, purity 99.5%; Alfa Aesar, MA, USA) were used as raw materials in this study. Al, B_4C and carbon were used for the synthesis of Al_3BC_3 and for the ABC system. By using stoichiometric composition to synthesize Al_3BC_3 (Al:B:C = 3:1:3 by molar ratio), the following compositions were selected for the present study: ZBABC5: ZrB_2 + 5 wt% Al_3BC_3, ZBABC10: ZrB_2 + 10 wt% Al_3BC_3, ZBABC15: ZrB_2 + 15 wt% A_3BC_3.

ZrB_2, Al, B_4C and carbon powers were ball-milled for 4 h in a polyethylene bottle using agate balls and ethanol as the grinding media. Then the slurry was homogenized again by sonication for dispersion by ultrasonic for 30 min, and was dried by rotate evaporation.

2.2. Densification

The power mixtures were loaded into a graphite mold (inner diameter 30 mm) lined with graphite foil and densified using SPS (Dr. Sinter 2020, Sumitomo Coal Mining Co., Tokyo, Japan) in vacuum (~6 Pa) at 1700° C for 10 min under an uniaxial pressure of 40 MPa (heating rate: 100° C/min). A 12 ms-on and 2 ms-off pulse sequence were used. The heating process was controlled using a monochromatic optical pyrometer that was focused on the hole of the side of the graphite mold. The sintering shrinkage of the specimen was analyzed by measuring the movement of the lower electrode (resolution 0.01 mm) which was connected to a computer to log the shrinkage curves.

2.3. Property analysis

The bulk densities of sintered samples were measured using Archimedes' method. The theoretical densities of the sintered specimens were calculated by the rule of mixture. The theoretical densities of Al_3BC_3 and ZrB_2 are 2.66 g/cm^3 and 6.09 g/cm^3, respectively [20]. Bending strength was measured by a three-point bending test (test bars 3 mm × 2 mm × 25 mm) with a span of 10 mm and a crosshead speed of 0.5 mm/min. Fracture toughness was measured by the single-edged notch beam (SENB) method (test bars 2.5 mm × 5 mm × 30 mm) with a span of 20 mm and a crosshead speed of 0.05 mm/min, the width of the notch being < 0.25 mm. Vickers hardness (HV) was measured by Vickers indentation (Wolpert 430SVD, USA) with a 98 N load applied for 15 s on polished sections. Minimum 5 specimens were tested for mechanical properties.

The microstructure and phase fraction of sintered specimens were analyzed by scanning electron microscopy (SEM, JEOL JSM-6700F, Tokyo) and X-ray diffraction analysis (XRD, XD-3, China) using Cu Kα radiation.

3. Results and discussion

3.1. Densification behavior

Fig 1 shows the densification curves during sintering of the ZrB_2–ABC compacts at 1700 °C. The initial became distinct with increasing the amount of the ABC additive. This observation was due to the plastic deformation of the aluminum particles at low temperature. The displacement curves of the ZrB_2–ABC samples were similar. Initial extension due to the heating of the graphite punches was followed by the moderate shrinkage. Subsequently, rapid densification occurred until the saturation of shrinkage. The sintering shrinkage behavior of the ZrB_2–ABC systems was similar with those of the systems densified by liquid phase sintering mechanism. As a consequence the sintering behavior of the ZrB_2–ABC could be classified into three stages according to the slope of the shrinkage curve: slow densification, fast densification, and solid-state sintering. The densification curves of the ZrB_2–ABC samples shift towards lower temperatures with increasing the amount of ABC sintering additive.

In the stage of slow densification, the rearrangement of particles took place in the compact. The onset temperature of shrinkage of the ZBABC10 and the ZBABC15 was

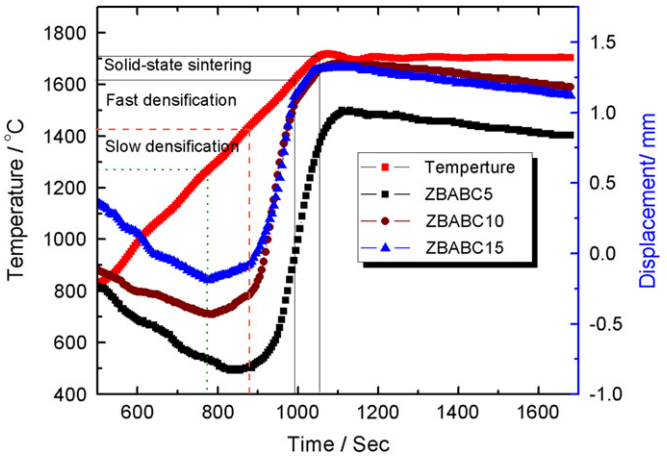

Fig. 1. Shrinkage of the ZrB_2–ABC ceramic composites during spark plasma sintering.

Table 1
Mechanical properties of the ZrB_2–ABC ceramic composites.

Sample	Relative density (%)	Fracture toughness (MPa $m^{1/2}$)	Flexural strength (MPa)	Vickers (GPa)
ZBABC5	97.6	5.55 ± 0.13	419 ± 32	19.6 ± 0.35
ZBABC10	99.3	5.94 ± 0.16	515 ± 26	18.7 ± 0.36
ZBABC15	99.5	6.17 ± 0.01	529 ± 6	14.9 ± 0.45

1243° C, which was about 30° C lower than that of the ZBABC5 sample. The beneficial of the ABC on the initial stage sintering was saturated above 10 wt%. During the second regime of fast densification, the shrinkage begins at about 1420° C. This stage was responsible for the majority of the total shrinkage. In the final stage of sintering, the shrinkage of the ZBABC10 and the ZBABC15 sample stopped immediately after heating to isothermal temperature. However, the shrinkage of the ZBABC5 sample progressed continuously at the early stage of isothermal heating.

The relative density of the ZBABC5 composite reached 97.6% at 1700° C (Table 1). The relative density of the ZBABC10 and the ZBABC15 composites reached nearly 100% at 1700° C (Table 1). The densification behavior of ZrB_2 was improved with increasing the amount of the ABC.

3.2. Microstructure analysis

Fig. 2 is the XRD patterns of the sintered specimens. The crystalline phases detected by X-ray diffraction in all samples were ZrB_2. Small peaks of Al_3BC_3 were detected in the specimens containing 10–15 wt% of the ABC. This indicated that Al_3BC_3 formed during densification by the reaction of the ABC.

Fig. 3(a) presents the fractured surfaces of the ZBABC5 sample. A subsequent SEM analysis confirmed that the level of porosity was lower than 3% (shown in Fig.1(a)). Small amount of pores were distributed at the grain boundary. The grain size was about 4–6 μm. The ZBABC10 and the ZBABC15 showed fine microstructure with less pores than the ZBABC5, as shown in Fig. 3(b) and (c). The grain size of the ZBABC10 was about 3–5 μm, which was larger than that of the starting ZrB_2 powders. The improvement of sinterability of ZrB_2 due to the ABC additive was associated with the formation of a liquid phase at high temperatures. It is known that Al has a low melting point of 660° C. Then, in the initial stage at a temperature just above 660° C, metal Al melted and other solid additives dissolved into the Al melt. The liquid phases spread and wetted solid grains. Zhang et al. [17] reported that Al vapor was possibly formed at high temperatures and further coated the solid powder surface, which can serve as a lubricant for particle rearrangement. Al and O enrichment in grain boundary was detected by EDS (shown in Fig. 3(d)), indicating that Al and oxides were

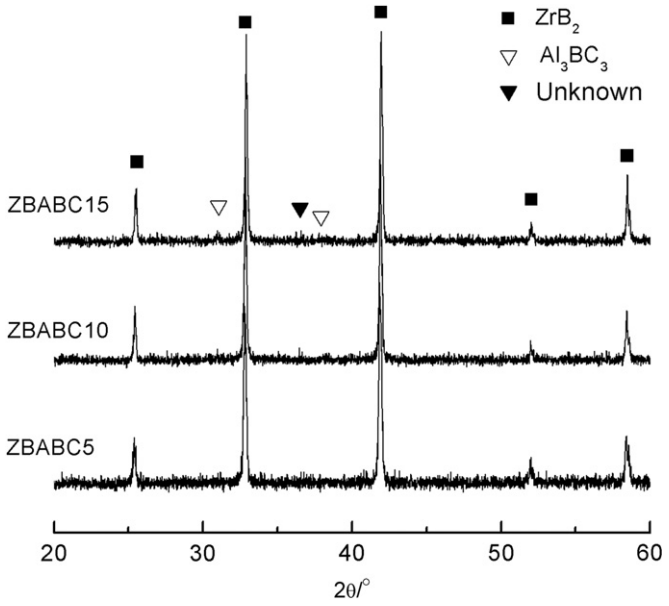

Fig. 2. XRD patents of the sintered ZrB_2–ABC ceramic composites by SPS at 1700° C.

dispersed in grain boundaries between ZrB_2 grains. B_2O_3 and Al_2O_3 films are present on the surfaces of ZrB_2 and Al particles, respectively. In the present study, B_2O_3 and Al_2O_3 can form a solution to prevent the evaporation of B_2O_3 during SPS and result in the formation of a stable liquid phase between the grains, therefore improving sinterability [21]. The sinterability was improved with increasing the amount of ABC. During the densification of SiC, the ABC are known to enhance boundary diffusion, thus facilitating densification [18].

3.3. Mechanical properties

The mechanical properties are summarized in Table 1. The hardness of the ZBABC5 was 19.6 ± 0.35 GPa, which decreased with the increasing amount of ABC. The hardness of the specimens was lower than the reported values (> 21 GPa) [1]. Because the hardness of Al_3BC_3 (11 GPa) is lower than that of ZrB_2 [22]. The room-temperature flexure strength of the ZrB_2–ABC composites was improved with increasing the ABC content from 419 MPa (ZBABC5) to 529 MPa (ZBABC15).

The fracture toughness of ZrB_2–ABC composites was higher than the reported results of ZrB_2 (3.5–4.2 MPa $m^{1/2}$) [1], and the value increased with ABC content from 5.55 MPa $m^{1/2}$ to 6.17 MPa $m^{1/2}$. In order to elucidate the toughening mechanisms, the propagation path of Vickers-indentation-induced cracks in the specimens were observed by SEM, as shown in Fig. 4. Crack deflection and crack bridging were observed in the ZBABC10 and the ZBABC15 samples, which increased resistance against crack propagation in the sample and consume more energy for separation of the fracture surface. Therefore, crack deflection and crack bridging were believed to be the

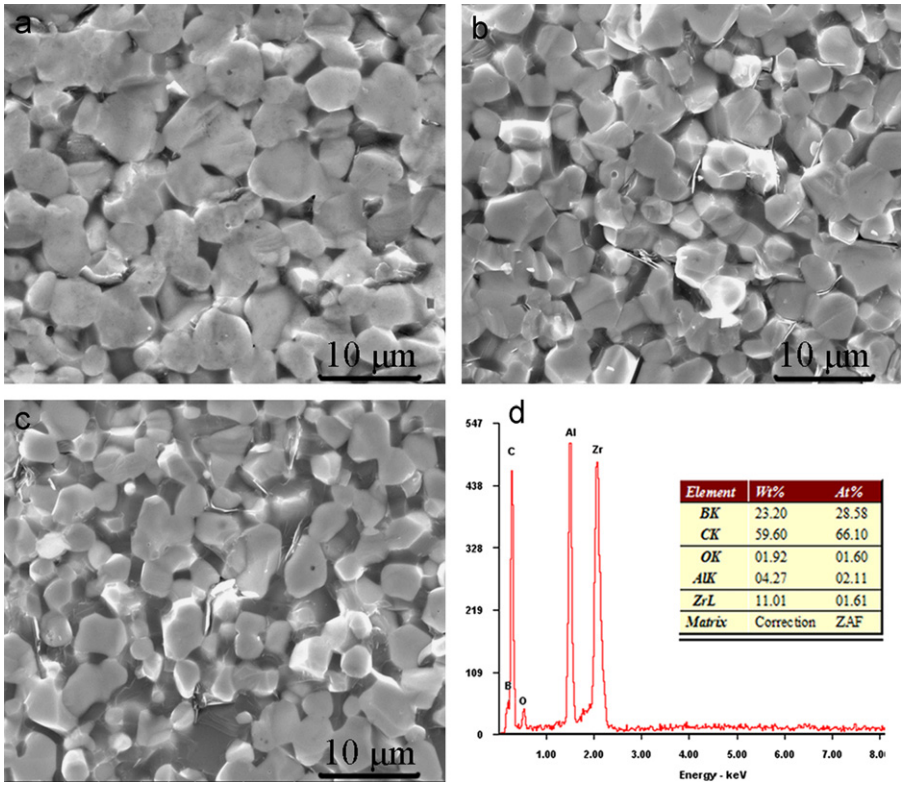

Fig. 3. SEM images of the fracture surface of the sintered ZrB_2–ABC ceramic composites ((a) ZBABC5, (b) ZBABC10, (c) ZBABC15) and EDS data of the grain boundary (d).

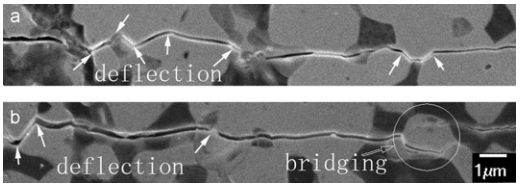

Fig. 4. SEM micrograph of the crack path on the polished and etched surface (a. ZBABC10 and b. ZBABC15).

primary toughening mechanism of ZrB_2 sintered with the ABC.

4. Conclusions

ZrB_2 ceramics have been densified by spark plasma sintering at 1700° C using Al, B_4C and carbon as the sintering additive. Al_3BC_3 formed during the sintering process played an important role in promoting densification and improving the sinterability of ZrB_2 ceramics. Both fracture toughness and flexural strength of ZrB_2 sintered with Al–B_4C–C additives increased with increasing the content of the additive. The observed toughening mechanisms were attributed to crack deflection and crack bridging.

Acknowledgments

The work was supported by the National Natural Foundation of China (no.51002142), the Specialized Research Fund for the Doctoral Program of Higher Education of China (20100471001) and the Development fund of State Key Laboratory of New Ceramics & Fine Processing of Tsinghua (KF09010).

References

[1] W.G. Fahrenholtz, G.E. Hilmas, I.G. Talmy, J.A. Zaykoski, Refractory diborides of zirconium and hafnium, Journal of the American Ceramic Society 90 (2007) 1347–1364.
[2] A.L. Chamberlain, W.G. Fahrenholtz, G.E. Hilmas, D.T. Ellerby, High-strength zirconium diboride-based ceramics, Journal of the American Ceramic Society 87 (2004) 1170–1172.
[3] P. Hu, Z. Wang, Flexural strength and fracture behavior of ZrB_2–SiC ultra-high temperature ceramic composites at 1800° C, Journal of the European Ceramic Society 30 (2010) 1021-1026.
[4] W.M. Guo, Z.G. Yang, G.J. Zhang, Effect of carbon impurities on hot-pressed ZrB_2–SiC ceramics, Journal of the American Ceramic Society 94 (2011) 3241–3244.
[5] H. Wang, C.A. Wang, X. Yao, D. Fang, Processing and mechanical properties of zirconium diboride-based ceramics prepared by spark plasma sintering, Journal of the American Ceramic Society 90 (2007) 1992–1997.
[6] X. Sun, W.B. Han, Q. Liu, ZrB_2-ceramic toughened by refractory metal Nb prepared by hot-pressing, Materials and Design 31 (2010) 4427–4431.
[7] H. Wang, D. Chen, C.A. Wang, R. Zhang, D. Fang, Preparation and characterization of high-toughness ZrB_2/Mo composites, International Journal of Refractory Metals and Hard Materials 27 (2009) 1024–1026.
[8] Z. Wu, Z. Wang, G. Shi, J. Sheng, Effect of surface oxidation on thermal shock resistance of the ZrB_2–SiC–ZrC ceramic, Composites Science and Technology 71 (2011) 1501–1506.

[9] Z. Wang, S. Wang, X.H. Zhang, P. Hu, W.B. Han, C.Q. Hong, Effect of graphite flake on microstructure as well as mechanical properties and thermal shock resistance of ZrB_2–SiC matrix ultrahigh temperature ceramics, Journal of Alloys and Compounds 484 (2009) 390–394.
[10] S.Q. Guo, Densification of ZrB_2-based composites and their mechanical and physical properties: a review, Journal of the European Ceramic Society 29 (2009) 995–1011.
[11] S.Q. Guo, Y. Kagawa, T. Nishimura, D. Chung, J.-M. Yang, Mechanical and physical behavior of spark plasma sintered ZrC–ZrB_2–SiC composites, Journal of the European Ceramic Society 28 (2008) 1279–1285.
[12] L.S. Walker, W.R. Pinc, E.L. Corral, Powder processing effects on the rapid low-temperature densification of ZrB_2–SiC ultra-high temperature ceramic composites using spark plasma sintering, Journal of the American Ceramic Society 95 (2012) 194–203.
[13] L. Zhang, D.A. Pejaković, J. Marschall, M. Gasch, Thermal and electrical transport properties of spark plasma-sintered HfB_2 and ZrB_2 ceramics, Journal of the American Ceramic Society 94 (2011) 2562–2570.
[14] S.H. Lee, Y. Sakka., H. Tanaka, Y. Kagawa, Wet processing and low-temperature pressureless sintering of SiC using a novel Al_3BC_3 sintering additive, Journal of the American Ceramic Society 92 (2009) 2888–2893.
[15] R. Yuan, J.J. Kruzic, X.F. Zhang, L.C.D. Jonghe, R.O. Ritchie, Ambient to high-temperature fracture toughness and cyclic fatigue behavior in Al-containing silicon carbide ceramics, Acta Materialia 51 (2003) 6477–6491.
[16] S.H. Lee, Low temperature pressureless sintering of SiC using an aluminum borocarbide additive, Journal of the American Ceramic Society 94 (2011) 2746–2748.
[17] X.F. Zhang, M.E. Sixta, L.C.D. Jonghe, Grain boundary evolution in hot-pressed ABC–SiC, Journal of the American Ceramic Society 83 (2000) 2813–2820.
[18] J.J. Cao, W.J. MoberlyChan, L.C. De Jonghe, C.J. Gilbert, R.O. Ritchie, in situ toughened silicon carbide with Al–B–C additions, Journal of the American Ceramic Society 79 (1996) 461–469.
[19] K.S. Cho, Z.A. Munir, H.K. Lee, Microstructure of spark plasma sintered silicon carbide with Al–B–C, Journal of Ceramic Processing Research 9 (2008) 500–505.
[20] S.H. Lee, Y. Sakka., H. Tanaka, Thermal stability of Al_3BC_3, Journal of the American Ceramic Society 92 (2009) 2172–2174.
[21] M. Hoch, Thermodynamic properties and phase diagrams of the binary systems B_2O_3–Ga_2O_3, B_2O_3-–Al_2O_3 and B_2O_3–In_2O_3, Journal of Alloys and Compounds 320 (2001) 267–275.
[22] S.H. Lee, H.D. Kim, S.C. Choi, T. Nishimura, J.S. Lee, H. Tanaka, Chemical composition and microstructure of Al_3BC_3 prepared by different densification methods, Journal of the European Ceramic Society 30 (2010) 1015–1020.